Chapter 2: Comparison of the Regimes Studied as Part of the FY-13 JRT

1.0 Database Motivation and Definitions

As part of the JRT2013 research activity, database has been contructed allowing comparisons between the various regimes discussed in this report. The motivation for this exercise was to i) assess progress relative to the goals of the JRT, ii) provide multi-machine context for the subsequent single facility reports, and iii) assist in guiding future experiments on DIII-D and NSTX-U, and potentially C-Mod. Brief descriptions of the various confinement regimes can be found in Chapter 1, with additional details in the facility report chapters.

This database includes equilibrium quantities from EFIT (or equivalent), such as the plasma current and toroidal field, parameters describing the plasma shape (R_0, a, κ, δ), and parameters describing the plasma energy content, such as the total stored energy and various measures of β. The database also contains a number of pedestal parameters, including most importantly the pedestal top T_e, n_e, and in some cases, T_i and Z_{eff}. Finally, a number of additional parameters, such as the line average density, auxiliary heating powers and global confinement multipliers are included. Note that edge turbulence/fluctuation data are not included in the database, as these data tend to be quite facility and even discharge specific.

For DIII-D, the regimes under consideration in the database include RMP H-mode, QH-mode, and I-mode examples. These DIII-D points appear as squares in the figures in this section. The pedestal parameters come from the standard post-shot fitting routines, not the specialized kinetic efit pedestal reconstructions utilized at other places in this report. Note that most of the I-mode points were collected as part of the JRT 2013 related experiments, and that additional data may be collected as part of the October 2013 DIII-D National Campaign.

The C-Mod data in these figures includes data from a large range of I-mode experiments. The pedestal parameters come from two different sets of analysis. One large data set uses the kinetic variable values taken at the 95% poloidal flux surface as representative of the pedestal top points; these ψ_N=0.95 values of density and temperature are scaled by 0.95 and 0.9, respectively. These scale factors come from a second smaller data set that additionally includes dedicated pedestal fits. The pedestal Z_{eff} is set to unity for these calculations.

The NSTX data comes from Enhanced Pedestal H-mode (EP H-mode) examples, and a limited number of cases where Edge Harmonic Oscillations (EHOs) have been observed. The pedestal fits utilized here are computed as a function of major radius, as the NSTX profile diagnostics are located on the device midplane. Note that, as described in Section 5, no NSTX regime has simultaneously achieved high confinement, complete elimination of large ELMs, and stationary conditions. The density is typically slowly rising in these discharges, and this should be borne in mind when inspecting the plots.

For more information on any of these topics, please see chapters 3-5, where the results from the individual machines are discussed in greater detail.

2.0 Comparisons Between Regimes Studied as Part of the 2013 JRT

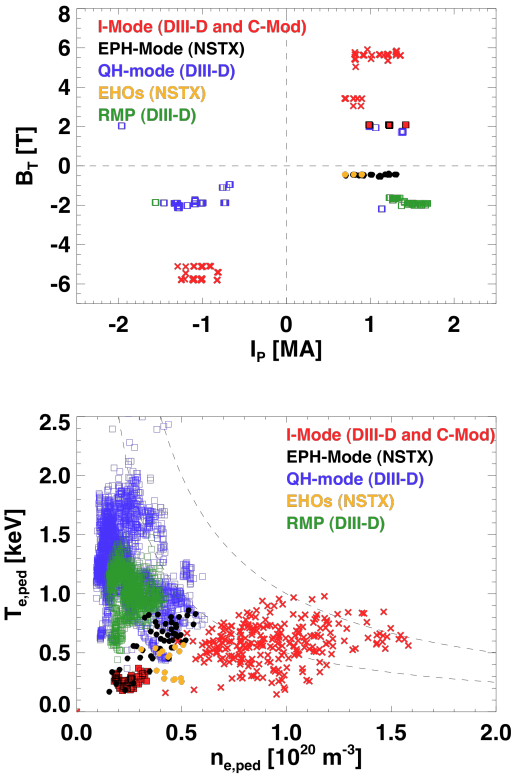

Fig. 2.1 Plots of (top) toroidal field vs. plasma current, and (bottom) the pedestal top temperature vs. the pedestal top density. NSTX data points are indicated as solid circles, DIII-D points by squares, and C-Mod points by the 'X' symbol.

Finally, the high-field Alcator C-Mod device has contributed data at toroidal fields of up to 5.9 T. Note the variations in

2.1 Comparisons of 0D Quantities

The first set of comparisons made with this database involve the dimensional parameters from the various devices, and are shown in Fig. 2.1. The top frame shows the current and field utilized for the various regimes. The NSTX data clusters around a field of 0.4-0.5 T and plasma currents in the range $700<I_P$ [kA]<1300. The DIII-D data operate at currents up to 2000 kA, and fields up to 2.2 T.

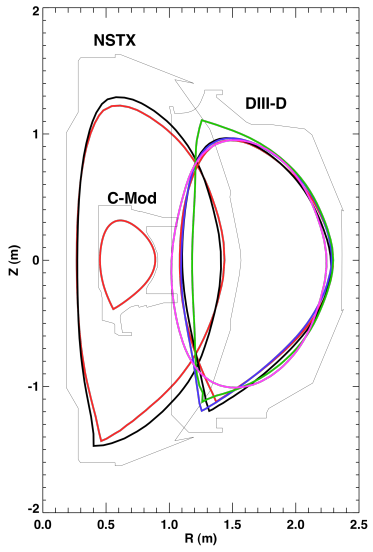

Fig. 2.2: Limiter and plasma boundaries for C-Mod, DIII-D, and NSTX. The plasma shapes shown are from discharges discussed in this report.

the sign of I_P or B_T, in order to i) change the ∇B drift direction relative to the direction of the dominant divertor, or ii) switch between dominant co-I_P or counter-I_P neutral beam injection.

The lower frame in Fig. 2.1 illustrates the absolute pedestal-top parameters for these discharges. As could be anticipated from the higher plasma current density, the C-Mod I-mode edge density is higher than the other devices, with values up to $1.5x10^{20}$ m^{-3}, and pedestal temperatures up to 1 keV. The DIII-D and NSTX pedestal densities are lower, and have comparable values of $1.5\text{-}6x10^{19}$ cm^{-3}. The DIII-D pedestals, however, have substantially higher temperature, with the best RMP cases approaching 1.5 keV and the hottest QH-mode cases exceeding $T_{e,ped}$ of 2 keV. The exception to this observation comes from the DIII-D I-mode cases, where pedestal top temperatures of 200-400 eV were common. As discussed in Section 4, the temperature pedestal evolution was often truncated by I→H mode transitions, often initiated by sawtooth heat pulses; the stated I-mode edge temperature and global confinement levels achieved to date may thus not represent the ultimate potential of the regime. Hyperbolas of the form $T_{e,ped}n_{e,ped}$=constant, corresponding to constant pedestal electron pressure, are also shown on the figure. These curves indicated that the high electron pedestal pressures occur in the hottest I-mode and QH-mode cases. The highest performance EP H-mode cases in Fig. 2.1 are also among the highest pedestal pressures observed in NSTX.

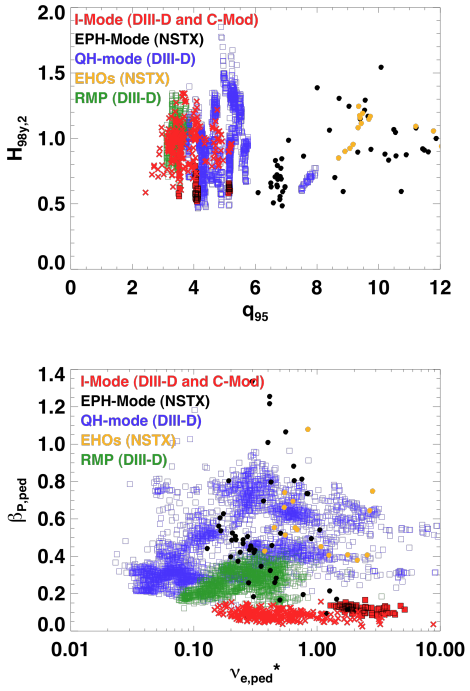

Fig 2.3: Plots from multi-machine database showing dimensionless global and pedestal parameters for the different plasma regimes in DIII-D, NSTX and C-Mod.

A final dimensional comparison is provided in Fig. 2.2, where the plasma cross-sections are shown for representative discharges from this study. DIII-D and NSTX have similar plasma cross-sectional areas, but different aspect ratios. DIII-D and C-Mod have similar aspect ratios, but different major and minor radii. Hence, in terms of geometry, field and current values, and pedestal parameters, the machines in this report scan a wide range of parameters.

A number of dimensionless parameters for these regimes are shown in Fig. 2.3, starting with $H_{98(y,2)}$ plotted against q_{95} in the upper frame. All of these regimes can produce confinement factor in excess of $H_{98(y,2)}$=1.2 at relevant normalized β, with the highest multipliers in select EPH- and QH-mode examples. RMP and C-Mod I-mode cases have achieved $H_{98(y,2)}$~1 confinement level at q_{95} levels appropriate for ITER Q=10 operation. Additionally, some QH-mode data points, obscured in the figure, have

achieved high-performance operation with q_{95}=3.2 and H~1, albeit with high levels of counter-NBI torque.

The bottom frame shows key dimensionless pedestal parameters, where the collisionality is calculated as. $\nu_{e,ped}^{*} = 0.012 n_{e,ped,20} Z_{eff} q_{95} R / \varepsilon^{3/2} T_{e,ped,keV}^{2}$ This figure shows that all these regimes have been extended into the ITER relevant $\nu_{e,ped}$*<1 regime envisioned by the annual target language, with QH-mode achieved over the largest range of pedestal collisionality among the regimes under consideration in this analysis. The DIII-D I-mode examples achieved to date have a somewhat higher pedestal collisionality than the C-Mod points in this regime, and future DIII-D I-mode work may attempt to reduce the collisionality in this regime further. With regard to the poloidal β values, the highest values occur in the NSTX scenarios and the QH-examples. Interestingly, the poloidal β for I-mode is similar for DIII-D and C-Mod, despite the quite different operating points in terms of field and current. Again, the limit in β to date has been set by input power or I→H transitions; as noted in Chapters 3 and 4, these I-mode pedestals were well below stability limits. Dedicated studies of the I-mode pedestal width in both DIII-D and C-Mod show that the width does not scale with $\beta_{P,ped}^{1/2}$, as has commonly been observed in H-mode, and that the absolute with tends to be larger than in H-mode.

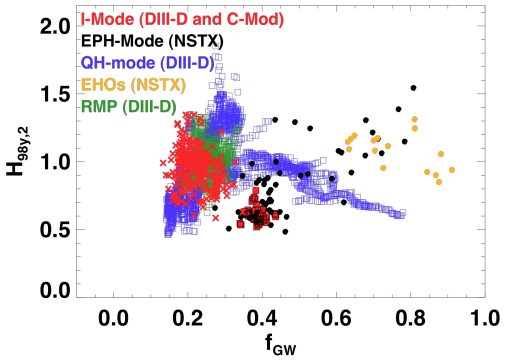

Fig 2.4:Plot of the confinement multiplier $H_{98(y,2)}$ vs. Greenwald Fraction, for the large database.

Finally, a recent focus of both I-mode and QH-mode studies has been to increase the density in these scenarios, towards the Greenwald fractions anticipated necessary for ITER [$f_{GW}=n_e/(I_P/\pi a^2)$, where the density is the line-average density in units of 10^{20} m^{-3}, the plasma current I_P is in MA, and the minor radius a is in meters]; progress towards achieving this goal is shown in Fig. 2.4. The achieved Greenwald fraction in these QH-mode regimes has now been increased to values of 0.8. These were achieved with gas puffing, and thus had a slow density ramp. However, all indications were that if the gas puffing were arrested, the density would have stabilized. The NSTX data also achieved good confinement at high density, including an EP H-mode case with H>1.5 with f_{GW}=0.8. The I-mode examples to date have been limited to lower Greenwald fractions, though still quite high values of absolute densities. However, experiments from C-Mod late in the FY12 campaign have had some success densifying the plasma after the L→I transition. Further increases appear possible, but have been precluded by lack of experimental time.

In summary, these plots and discussion show that:

- As envisioned in the target language, the three devices under consideration explore complementary portions of the achievable tokamak operating space.

- ITER relevant confinement and collisionality have been achieved in these various regimes.
- The prospects of achieving these regimes at the desired densities have been improved by recent experiments.
- The poloidal-β values of the DIII-D and C-Mod I-mode pedestals are similar, despite the vastly different absolute parameters. In any given machine, the I-mode pedestal has a larger width than of H-mode plasmas.

2.2 Comparisons of Key Physics Characteristics

Beyond these 0D comparisons, a number of common and divergent features have been noted when comparing the critical physics elements of these regimes.

Operating Points in Peeling-Ballooning Space: The macrostability of the edge plasma is generally considered to be constrained by current-driven low-n peeling modes and pressure driven intermediate-n ballooning modes. When these limits are crossed, an ELM is believed to occur. Studies described in this JRT report show that although the C-Mod Type-I ELMy H-mode cases are near the ballooning portion of this boundary, the I-mode cases tend to be far from any boundary; this provides justification for the statement above that there may be room to further increase the I-mode pedestal performance. The NSTX cases with EHOs, on the other hand, have been recently found to reside near the peeling boundary, as do the QH-mode examples. Mechanisms to potentially externally stimulate these presently week EHOs in NSTX-U are discussed in Chapter 5.

Role of Edge Rotation and Rotation Shear: It is clear that the edge rotation plays a role in many of these regimes. The edge rotation-shear plays a key role in determining the onset condition for the EHO in the QH-mode plasmas; this rotation shear is believed to destabilize low-n peeling modes, which saturate as the EHO. There is some evidence that there are optimal values of the rotation shear in NSTX for achieving EHOs as well, though this result is more speculative. However, these recent studies have shown that the edge rotation shear plays a key role in providing the reduced transport in the NSTX EP H-mode. Finally, it appears likely that the edge rotation plays a role in the screening physics during RMP application. Hence, developing a self-consistent understanding of edge momentum generation and transport, including the interaction and damping of flows by internally and externally generates 3D fields, is critical for the extrapolation of these regimes.

Edge Fluctuations and Particle & Impurity Transport: Recent experiments have shown that edge fluctuations play a key role in flushing particles and impurities in stationary ELM free regimes. DIII-D results using fluorine as a traces gas have found that the EHO can flush impurities more efficiently than ELMs, while C-Mod results have shown that the edge particle flux is proportional to the amplitude of the WCM. These results increase confidence in the ability of these confinement regime to support stationary operation in future devices.

External Torque Input: These studies have shown that the I-mode regime is accessible with both no external momentum input (ICRH plasmas in C-Mod), and with co-injected neutral beams (DIII-D), and that some pedestal parameters are similar with these two heating systems. Continued effort has been dedicated to generate low q_{95} QH-mode plasmas at ITER relevant torque, though locked mode formation remains problematic, and improved error field correction strategies will likely be implemented to mitigate this problem.

These physics element are discussed in greater detail in the following facility chapters.